AUTHOR(S):

Nishikawa, Hayato; Nakata, Eiji; Nakano, Shun; Nakajima, Takashi; Morii, Takashi

Influence of polymer molecular weight on the properties of in-situ synthesized silver-methylcellulose nanocomposite films with a CO₂ laser

Hayato Nishikawa, Eiji Nakata, Shun Nakano, Takashi Nakajima*, and Takashi Morii

Institute of Advanced Energy, Kyoto University, Gokasho, Uji, Kyoto 611-0011, Japan

ABSTRACT

We investigate the influence of polymer molecular weight on the properties of silver-methylcellulose (Ag-MC) nanocomposite films synthesized by the irradiation of a CO_2 laser. Although the reduction power of MC with a smaller molecular weight turns out to be stronger than that with a larger molecular weight in the solution phase, we do not see such a clear difference when MC is in the matrix phase. For the 30 sec irradiation at the laser power of 0.8 W, the size of Ag nanoparticles (NPs) in the two types of MC matrix is similar, and it is about 30 nm. However, for the longer irradiation time at the same laser power, aggregation of Ag NPs set in, and it is more serious for the Ag-MC film with MC of larger molecular weight. We also carry out the antibacterial test with the Ag-MC films, and find that the Ag-MC film synthesized at the lower laser power and shorter irradiation time generally exhibits a stronger antibacterial effect.

Keywords

silver nanoparticles; methylcellulose; nanocomposite; antibacterial activity; laser

*E-mail address: nakajima@iae.kyoto-u.ac.jp (Takashi Nakajima)

ORCID iD: https://orcid.org/0000-0003-4136-5383

Introduction

In recent years metal-polymer nanocomposites have continuously drawn lots of attention due to their potential applications in various fields [1-3]. The role of the metallic component as a filler is to improve the property of the polymer matrix or add new functions to them. In many cases synthetic polymers are used for the matrix because they already have nice properties, while noble metal nanoparticles (NPs) are used for the filler because they have good mechanical, electrical, optical, and catalytic properties.

There are many reports on the synthesis of metal-polymer nanocomposites, and the developed synthesis methods can be classified into the two categories, i.e., ex-situ [4] and in-situ methods. In the ex-situ methods the separately prepared metal NPs are dispersed into the polymer solution, and the mixed solution is spin-coated or cast on a substrate to make nanocomposite films. Although this is a very straightforward method, obtaining nanocomposite films with a high number density of metal NPs is difficult, because aggregation can take place. In the in-situ methods metal NPs are produced in the polymer matrix in various ways such as chemical reduction [5, 6], photoreduction [7–10], microwave reduction [11], thermal reduction [12], etc. The typical photoreduction method employs a UV lamp [7, 9] or UV laser [8, 10] to induce radicals of additives, and those radicals promote reduction in the polymer matrix. The thermal reduction is carried out in an electric furnace [12] at the temperature of 80~120 °C. As a new alternative, we have recently demonstrated the rapid in-situ synthesis of polymer-metal nanocomposite films using a CO_2 laser [13], where the role of the CO_2 laser is to heat the glass substrate through which the temperature of the polymer film also increases, and this promotes the reduction of metallic ions in the polymer matrix. In this sense our method is somehow similar to thermal reduction.

Cellulose is one of the polysaccharides, and the most abundant natural polymer on earth. Moreover, it is biodegradable, biocompatible, renewable, and nontoxic. Although these properties imply that cellulose can be an ideal material as a matrix of nanocomposites [14–16], there still remains a difficulty that cellulose is insoluble in water and most of the organic solvents, because the reactive hydroxyl groups in a cellulose molecular chain form the hydrogen bonds with the adjacent cellulose molecular chains and becomes practically inert. As a result, cellulose is often used in the forms of bundles such as cellulose nanocrystals or cellulose nanofibers [17–24]. However, the derivatives of cellulose such as methylcellulose (MC), carboxymethyl cellulose (CMC), and aminocellulose (AMC) exhibit good solubility in

water while acetylcellulose (AC) is soluble in acetone, and they can be conveniently used for the matrices of metal-polymer nanocomposites, as reported with MC [25–33], CMC [34–37], AMC [38], and AC [39].

Knowing that most of the polymer-based nanocomposites in the literature deal with the polymers with certain single average molecular weights, we address the question: "How are the properties of polymer-metal nanocomposites influenced by the molecular weight of employed polymers?" Related to this question we are aware that the synthesis of Ag NPs using the solutions of polyethylene glycol (PEG) with different molecular weights has been studied to clarify the influence of molecular weight of employed PEG on the properties of Ag NPs [40]. Since there is a growing interest for the use of cellulose derivatives as environmentally friendly materials the influence of its molecular weight on the properties of synthesized nanocomposites has to be clarified.

The aim of this work is to investigate the influence of polymer molecular weight of MC on the properties of Ag-MC nanocomposite films synthesized by the irradiation of a CO_2 laser [13] . Through the synthesis and characterization of Ag-MC films using MC with different molecular weights (which are often labeled in terms of viscosity, cP), we find that the choice of MC with different molecular weights results in the different optical and morphological, and antibacterial properties of the synthesized films even if the same laser power and irradiation time are employed.

Materials and Methods

Materials

We purchase two kinds of MC (viscosities of 2% solution at 20 °C are 15 cP and 400 cP with average molecular weights of 14,000 and 41,000, respectively, while the methoxy substitution and the degree of substitution are 29.5±2 % and 1.7±0.2, respectively, for both MCs, as all those data supplied by the manufacturer), polystyrene (PS) (molecular weight of 350,000), silver nitrate ($AgNO_3$, 99.999%), and silver acetate ($AgCH_3COO$, 99.999%) from Sigma-Aldrich, and toluene from Wako Pure Chemical industries Ltd. All reagents are analytical grade and used as received without further purification. The glass substrates used in our study are borosilicate microscope cover glass (18 mm×18 mm×0.15 mm, Matsunami Co.). Hereafter we will call MC (15 cP) and MC (400 cP) as MC15 and MC400, respectively. *Escherichia coli* (*E. coli*) DH5α competent cells are obtained from TaKaRa Bio Inc.

Laser

For the in-situ synthesis of Ag-MC films we employ a CO_2 laser at 10.6 μm (AL30P, Access Laser Co., maximum peak power 60 W, pulse duration 100-400 μs depending on the laser power, repetition rate 2.5 kHz). Although its output is in the pulsed mode, the irradiation may be considered to be in the quasi-CW mode, since the pulse duration is comparable to the pulse interval, which is 400 μs at the 2.5 kHz repetition rate. The CO_2 laser power is measured with a power meter (Pronto-250, Gentec-EO Co.) at the position of the polymer film. The laser beam diameter is ~8 mm (FWHM) with a Gaussian spatial profile at the position of the film. As a result the irradiated laser power on the film is different at the different position, and this influences the film properties. Although it is technically possible to convert the Gaussian beam profile to the flat-top one using a commercial beam shaper we do not use it in this work, and perform all the analysis at the center of the irradiated area on the film.

Synthesis of Ag-MC films

We mix 0.125 g of MC15 in 2.5 mL of highly purified water at 80 °C for 1 hour with continuous stirring, and then, gradually cool it down to the room temperature (20 °C). After that we store the solution in a refrigerator (-20 °C) overnight to obtain the MC15 solution. Then, we take out the MC15 solution from the refrigerator, and mix it with a separately prepared 0.47 M $AgNO_3$ solution which contains 0.08 g of $AgNO_3$ and 1.0 mL of water to obtain the $AgNO_3$-MC15 solution. The 500 μL of $AgNO_3$-MC15 solution is spin coated on a glass substrate at 500 rpm for 5 sec and then at 1000 rpm for 30 sec. The spin-coated $AgNO_3$-MC15 film is dried in a dark place in air at room temperature for 24 hours. $AgNO_3$-MC400 films are prepared in a similar way with the same wt% of MC in the solution. The only difference is that the employed speed of spin coating for the $AgNO_3$-MC400 films is 500 rpm for 5 sec and then 2000 rpm for 30 sec, otherwise the $AgNO_3$-MC400 films come out to be much thicker than the $AgNO_3$-MC15 films. This is because the viscosity of the MC400 solution is much higher than that of the MC15 solution at the same wt% concentration of MC. To check the film thicknesses we employ the atomic force microscope (VN-8010, Keyence), and find that they are 440 and 820 nm, respectively, for the $AgNO_3$-MC15 and $AgNO_3$-MC400 films. After the thickness check we irradiate the $AgNO_3$-MC films with the CO_2 laser (beam diameter ~10 mm at the film position) at the laser power of 0.8 or 1 W for 30, 60, or 90 sec to synthesize Ag-MC films. Upon laser irradiation the film temperature rapidly increases, and within 60 sec irradiation the

film temperature (measured by a thermocouple with a 1 mm diameter head) reaches 130 and 150 °C at the laser power of 0.8 and 1 W, respectively.

Characterization

To obtain the optical properties of the samples in the UV~visible range, we employ a compact CCD spectrometer (USB2000+, Ocean Optics). The film samples (i.e., Ag-MC15 and Ag-MC400 films) are directly placed in front of the spectrometer, while the solution samples (i.e., $AgNO_3$-MC15 or $AgNO_3$-MC400 solutions) are put in an acrylic cell (12.5 mm × 12.5 mm × 45 mm, optical path=10 mm) as shown in Fig. 1(a), and placed in front of the spectrometer for the UV-vis measurements. To characterize the film morphologies we employ a scanning electron microscope (SEM) (JSM-6500FE, JEOL) at 5 kV. Since the pure MC15 and MC400 films without $AgNO_3$ show the structureless SEM images even after laser irradiation, we can confidently say that any surface structure we can see on the Ag-MC films by SEM essentially reflect the shapes and sizes of in-situ synthesized Ag NPs at the film surface. To investigate the possible modification of the vibrational modes of MC matrix as a result of the formation of Ag NPs we employ Fourier Transform Infrared Spectroscopy (FTIR) (FT/IR-6200, JASCO). However, the borosilicate cover glass substrates are completely opaque for the mid-IR wavelength of 1000-4000 cm^{-1}, and we cannot use them as substrates for the FTIR measurement. Therefore, only for the FTIR measurements we introduce a sacrificial PS layer between the cover glass substrate and Ag-NO_3 film, irradiate the CO_2 laser, peel off the synthesized Ag-MC+PS film from the substrate, and dissolve the PS layer in toluene to obtain the free-standing Ag-MC film, which is mounted in the sample holder for the FTIR measurement.

Antibacterial test

To investigate the antibacterial properties of the Ag-MC films we perform the agar diffusion test against *E. coli* [41]. Briefly, fully grown *E. coli* is diluted with a Luria-Bertani (LB) medium and grown again until the optical density of 1.2 at 600 nm is reached. Then, the bacterial suspension is applied on the surface of a nutrient agar plate. The Ag-MC films on the glass substrates are cut into the size of 4 mm × 4 mm around the irradiation center to ensure the homogeneity of the synthesized films, and placed upside down on the agar plate. Finally, the agar plates are incubated at 37 °C for 24 hours. The antibacterial properties of the Ag-MC films synthesized under the different laser powers and irradiation times are evaluated from the inhibited area around the 4 mm × 4 mm Ag-MC films.

Results and Discussions

Reduction power of methylcellulose

To start with, we test the reduction power of MC itself. For this purpose we prepare the two sets of AgNO$_3$-MC15 and AgNO$_3$-MC400 solutions as described in 2.3, and place them in
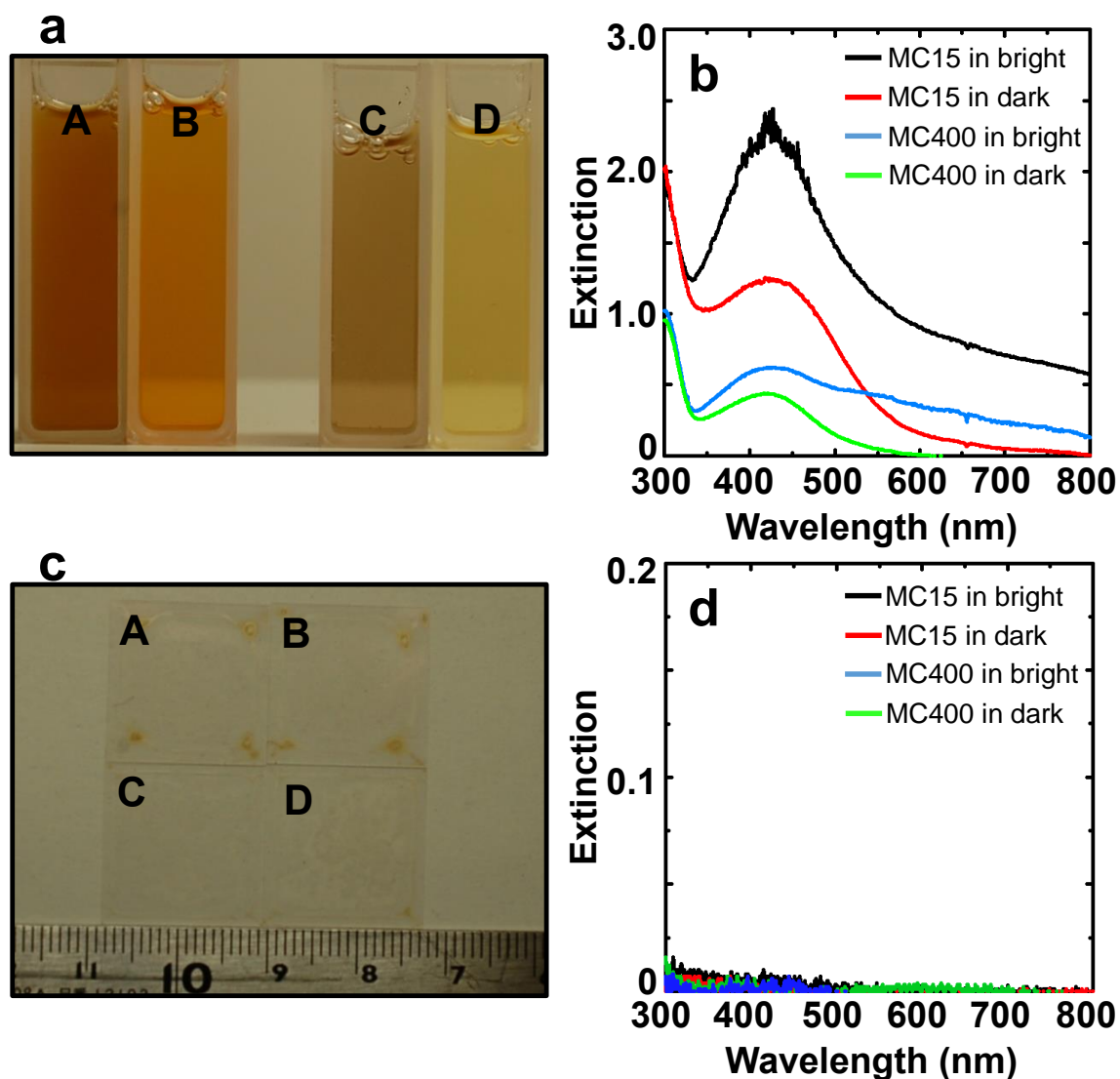

Figure 1 (a) Comparison of the reduction power of MC15 and MC400. A and B (C and D) represent the photos of the AgNO$_3$-MC15 (AgNO$_3$-MC400) solutions stored in bright and dark places for 24 hours, respectively. (b) UV-vis spectra of the corresponding solutions shown in (a). (c) Photos of the Ag-MC15 and Ag-MC400 films prepared by spin-coating the 24 hour-stored AgNO$_3$-MC15 and AgNO$_3$-MC400 solutions on the substrates. (d) UV-vis spectra of the corresponding films shown in (c).

bright and dark places at room temperature for 24 hours. The photos of the solutions after 24 hours are shown in Fig. 1a. As the reduction of Ag$^+$ ions proceeds the initially colorless

(transparent) AgNO₃-MC solution gradually changes to yellow and then to darker yellow. This color change is fastest for the AgNO₃-MC15 solution (Fig. 1a) stored in the bright place, and slowest for the AgNO₃-MC400 solution stored in the dark place. From the UV-vis spectra shown in Fig. 1b we confirm that the origin of the yellow color is due to the presence of the peaks at around 420 nm, which is a surface plasmon resonance (SPR) of Ag NPs. It is clear that the reduction, although very slow, proceeds even in the dark place, and the reduction power of MC15 is stronger than that of MC400. Now, those solutions are spin-coated on the glass substrates, and then dried in a dark place for another 24 hours. As shown in Fig. 1c the prepared films are practically transparent to the naked eye, since the film thickness is no more than a few hundred nm. Indeed, the UV-vis spectra of those films hardly show the SPR (Fig. 1d).

UV-vis spectra

In Figs. 2a and 2b we show the UV-vis spectra of Ag-MC15 films after the laser irradiation times of 0, 30, 60, and 90 sec at the laser powers of 0.8 and 1 W, respectively. From Fig. 2a we notice that the SPR of Ag NPs appears at around 400 nm [4, 5, 12] after the 30 sec irradiation, and it is far stronger than that we have seen in Fig. 1d. This means that the Ag-MC15 film with
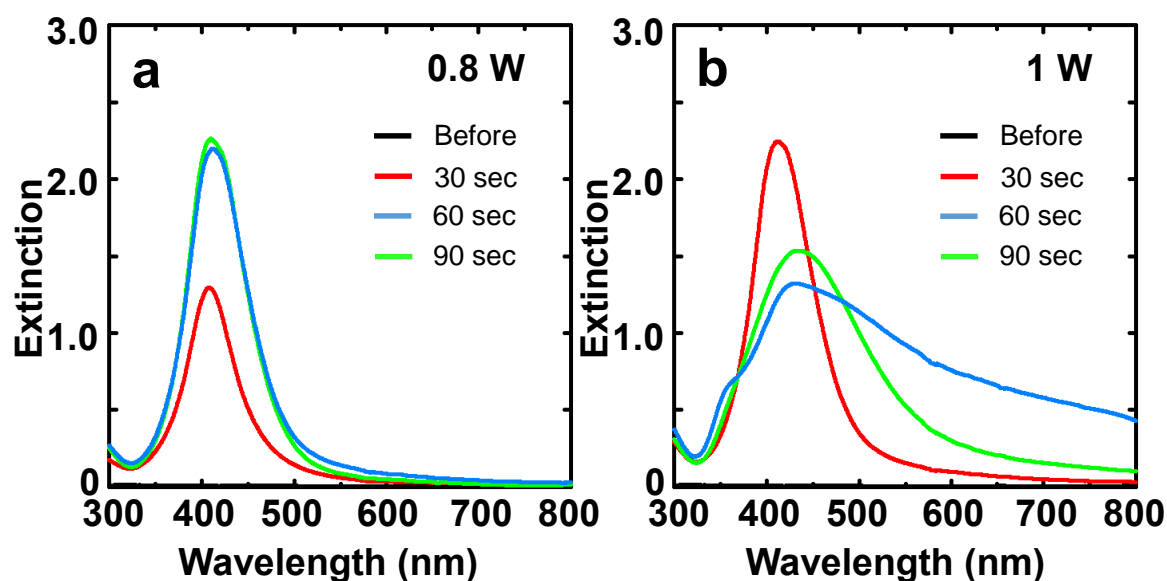

Figure 2 UV-vis spectra of the Ag-MC15 films synthesized at the different laser powers and irradiation times. Employed laser powers are (a) 0.8 W and (b) 1 W, respectively.

a tremendous number of Ag NPs has been in-situ synthesized through the reduction of Ag⁺ ions in the MC15 matrix. After the 60 sec irradiation the height of SPR grows, but the difference of the shape and height of SPR after the 60 and 90 sec irradiations are very small. This implies that practically all Ag⁺ ions in the MC15 matrix have been reduced to Ag NP

during the 60 sec irradiation at 0.8 W, and thereafter very little change occurs until the CO_2 laser is turned off at 90 sec. However, when the laser power is increased to 1 W the behavior of the UV-vis spectra turns out to be different, as shown in Fig. 2b. At the laser power of 1 W the 30 sec irradiation turns out to be sufficient to reduce practically all Ag^+ ions in the MC15 matrix, since the UV-vis spectrum after the 30 sec irradiation at 1 W (Fig. 2b) is almost the same with those after the 60 and 90 sec irradiations at 0.8 W (Fig. 2a). Further irradiation (60 sec) at 1 W broadens the SPR and the peak shifts to the longer wavelength side. These observations imply that the size of Ag NPs becomes more polydisperse with the larger average size of Ag NPs. After the 90 sec irradiation at 1 W the tail of the SPR at the long wavelength side lifts up from the baseline, suggesting that the significant aggregation of Ag NPs has taken place. Note that these changes do not happen at the laser power of 0.8 W (Fig. 2a), since, due to the lower film temperature at 0.8 W, the mobility of the reduced Ag NPs in the MC15 matrix is not sufficient to meet another Ag NPs in the neighborhood to aggregate. At the laser power of 1 W, however, the Ag NPs which have been reduced in the MC15 matrix at the earlier time during the laser irradiation can meet another Ag NPs to aggregate and become larger NPs, since, due to the higher film temperature at 1 W, the reduced Ag NPs can move more distance in the softer MC15 matrix.

Similar results are shown in Figs. 3a and 3b for the Ag-MC400 films. Although the reduction power of MC400 solution is somehow weaker than that of MC15 solution (Fig. 1a), the MC400 matrix under the laser irradiation at 0.8 W can sufficiently reduce Ag^+ ions. Presumably, this is because more water molecules remains in the MC400 matrix even after the 24 hour dry, and accordingly the mobility of Ag atoms/clusters/NPs during the CO_2 laser irradiation is higher in the MC400 matrix with, which promotes the reduction. In other words the lower reduction power of MC400 itself is compensated by the presence of residual water molecules in the MC400 matrix to improve the reduction power to be comparable with that of MC15. However, the SPR's in Fig. 3a are all slightly broader than those in Fig. 2a, because the size of Ag NPs in the Ag-MC400 films after the irradiation at 0.8 W is larger as a result of aggregation. This interpretation is confirmed by the longer tails and broader widths of SPR's shown in Fig. 3a compared with those shown in Fig. 2a. At the laser power of 1 W (Fig. 3b) the distortion of SPR for the Ag-MC400 films is more eminent than that for the Ag-MC15 films (Fig. 2b), because the MC400 matrix is more viscous than the MC15 matrix at the same film temperature (i.e., same laser power), and accordingly the rapidly synthesized NPs at 1 W
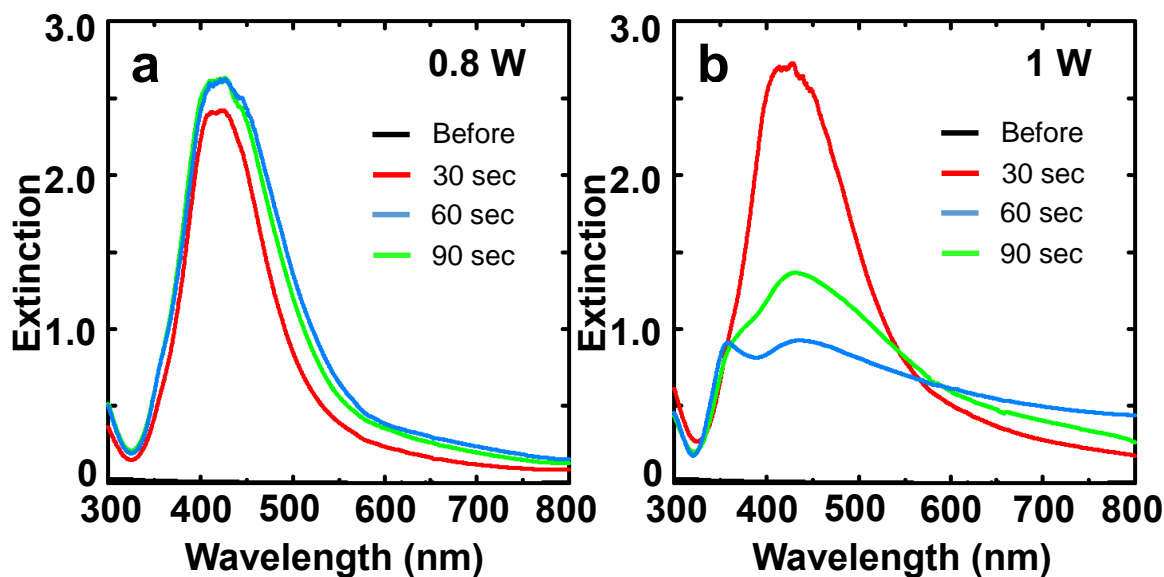
Figure 3 Similar to Fig. 2 but for the Ag-MC400 films.

cannot so much diffuse. As a result aggregation of Ag NPs is more likely to occur in the MC400 matrix.

Surface morphology

Now, to have a better picture for the in-situ formation of Ag NPs in the MC matrix we study the morphology of Ag-MC films. Under the laser power of 0.8 W the morphologies of Ag-MC15 (Ag-MC400) films are similar for both 30 and 90 sec irradiations (not shown here), and the average sizes of Ag NPs are 29.4 and 29.4 nm (30.4 and 31.5 nm), respectively, while their size distributions are all similar to that shown in Fig. 4a. Figs. 4a and 4b show the SEM images of the Ag-MC15 films synthesized by the 30 and 90 sec irradiations at 1 W, respectively. We notice that many Ag NPs are exposed out of the film surface. To obtain the size distributions of Ag NPs we employ the ImageJ software to analyze the SEM images, and the results are shown in Figs. 4c and 4d. The average size of Ag NPs after the 30 sec irradiation is 30.6 nm, while it becomes 37.6 nm after the 90 sec irradiation. Moreover, we notice that the size distribution of Ag NPs after the 90 sec irradiation (Fig. 4d) is broader than that after the 30 sec irradiation (Fig. 4c). This is consistent with the change we observe in the UV-vis spectra (Fig. 2b): The UV-vis spectrum after the 90 sec irradiation is broader than that after the 30 sec irradiation, and the former has a long tail in the long wavelength side, indicating that the size distribution is broader and the aggregation of Ag NPs takes place during the 90 sec irradiation at 1 W.
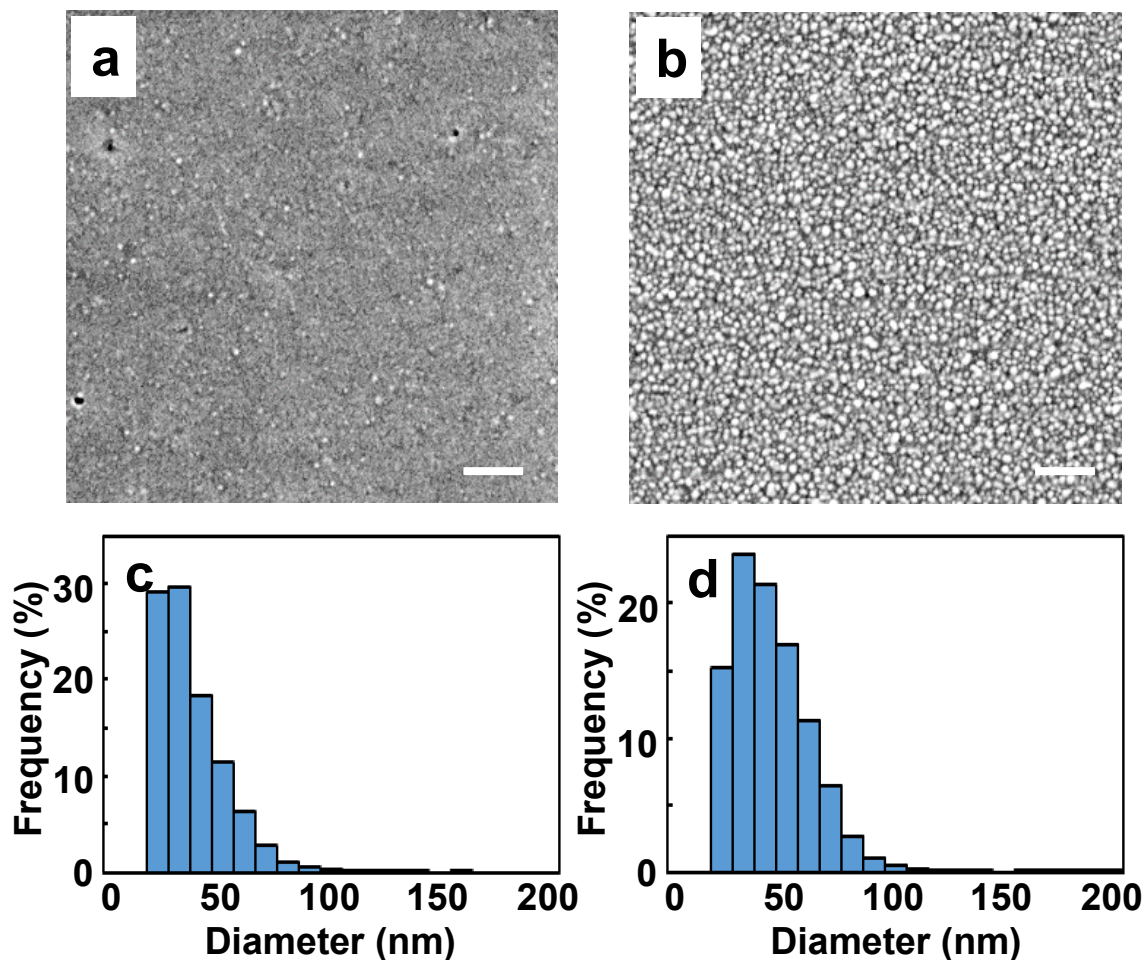
9

Figure 4 SEM images for the Ag-MC15 films synthesized by the (a) 30 sec and (b) 90 sec irradiations at 1 W. Size distributions of Ag NPs shown in (a) and (b) are presented by the histograms in (c) and (d), respectively. The scale bars in (a) and (b) represent 500 nm.

Similar results for the Ag-MC400 films are shown in Fig. 5. From the comparison of Fig. 5a with Fig. 4a we notice that, after the 30 sec irradiation at 1 W, the average size of Ag NPs in the Ag-MC400 film (29.8 nm) is similar to that (30.6 nm) in the Ag-MC15 film, and the size distributions are also similar, as we see in Figs. 5c and 4c. Interestingly, after the 90 sec irradiation at 1 W, notable aggregation of Ag NPs is observed in the Ag-MC400 film (Fig. 5b), and consistently the size distribution of Ag NPs is very broad (Fig. 5d). Note that the results are very different for the Ag-MC15 films (Figs. 4b and 4d). As already mentioned above, this is presumably because the viscosity of MC400 matrix is higher than that of the MC15 matrix at the same film temperature, which results in the more chance for the in-situ growing NPs to meet the adjacent NPs to aggregate. Although the Ag NPs after the 90 sec irradiation at 1 W is strongly distorted and far from the spherical shape, we dare to make a rough estimation of the average sizes of Ag NPs using ImageJ, and they are 29.8 and 165 nm after the irradiation times
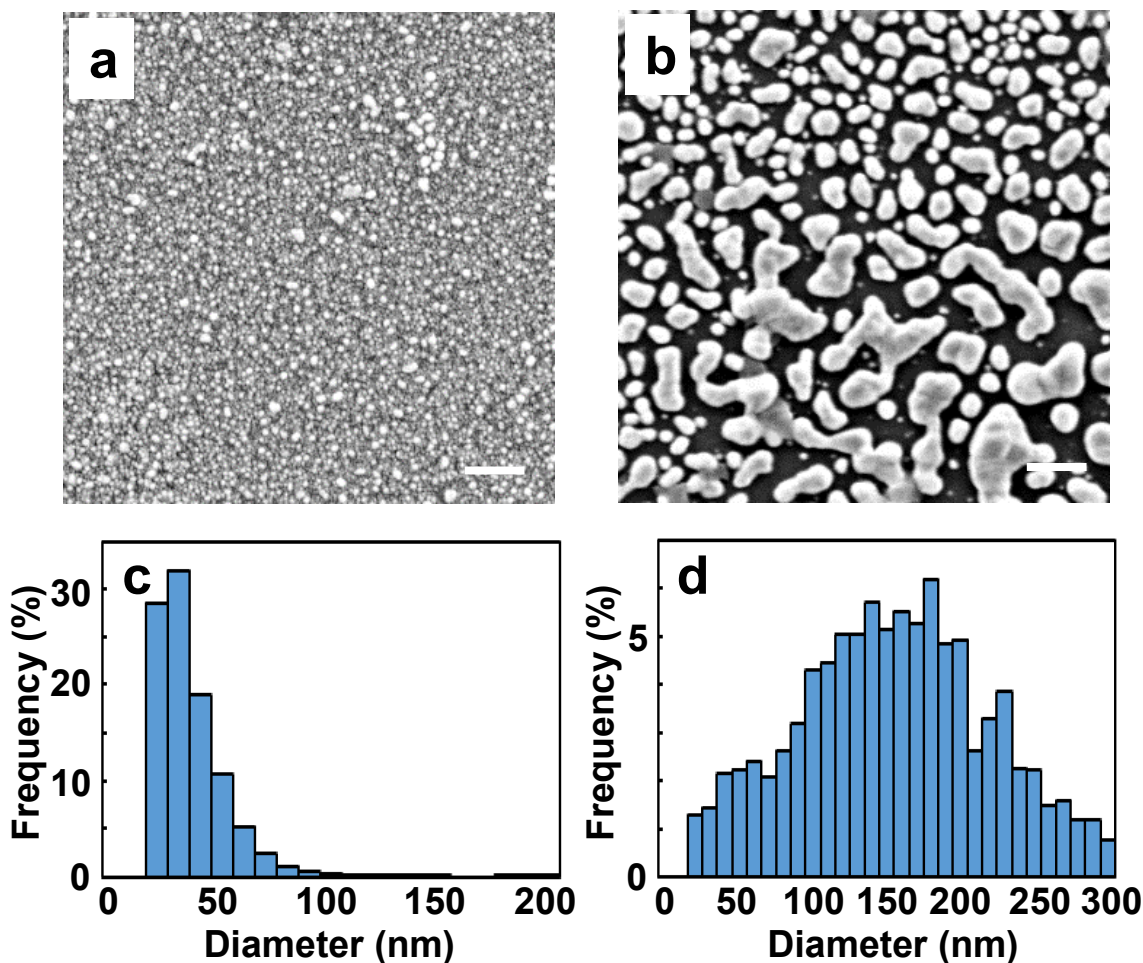
Figure 5 Similar to Fig. 4 but for the Ag-MC400 films.

of 30 and 90 sec, respectively. These findings are qualitatively consistent with what we have already inferred from the UV-vis spectra shown in Fig. 3.

FTIR spectra

Now, we take the FTIR spectra to gain some insights about the interaction in the Ag-MC films. The results are summarized in Fig. 6. The peaks at about 3469 cm^{-1}, 2921 cm^{-1}, and 1081 cm^{-1} are characteristic for the MC molecules, and they are the O-H stretching mode, asymmetric C-H stretching mode of pyranoid ring, and C-O-C stretching mode from gluocosidic units, respectively [42]. Those modes appear in all the FTIR spectra of pure MC15, Ag-MC15, pure MC400, and Ag-MC400 films (Figs. 6a-6d) with some slight difference in shape and energy, which indicates the presence of interactions between the Ag NPs and MC matrix. More
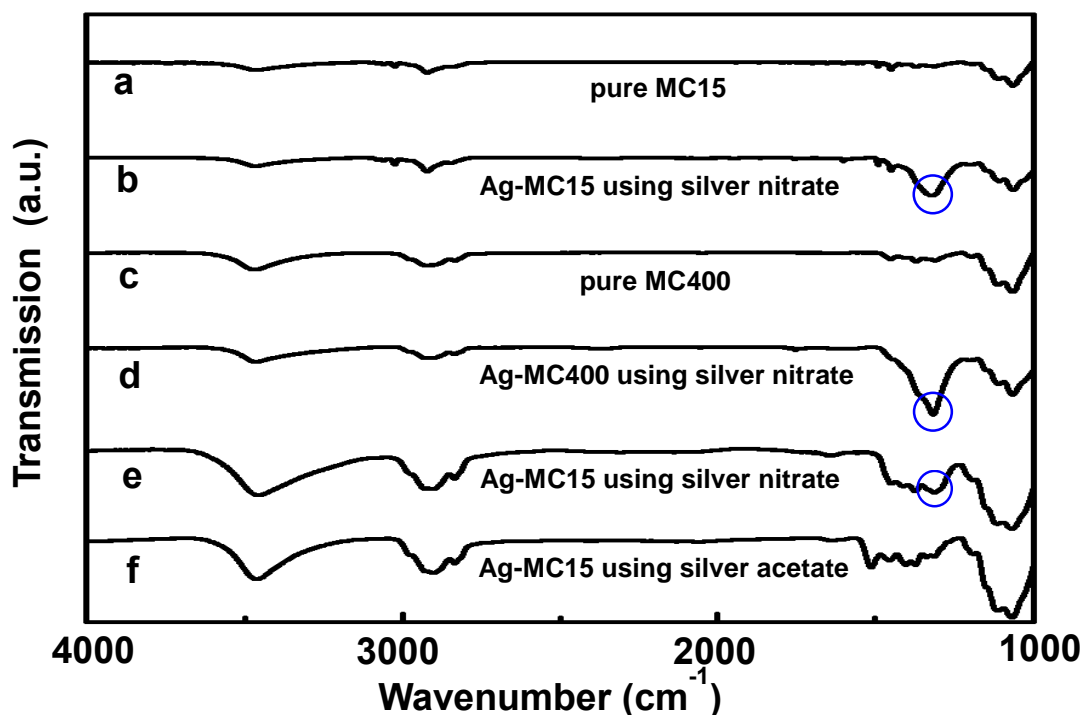
Figure 6 FTIR spectra of the free-standing (a) pure MC15 film, (b) Ag-MC15 film synthesized by 90 sec laser irradiation at 1W, (c) pure MC400 film, and (d) Ag-MC400 film synthesized by 90 sec laser irradiation at 1 W. Graphs (e) and (f), respectively, represent the FTIR spectra of the free-standing Ag-MC15 films using silver nitrate and silver acetate with the same but much lower concentration employed for (b) and (d).

interestingly, an additional peak appears at 1318 cm^{-1} (circled in Figs. 6b and 6d) only in the Ag-MC15 and Ag-MC400 films. To find the origin of this peak we additionally synthesize the Ag-MC15 film using silver acetate instead of silver nitrate as a precursor of Ag NPs. Solubility of silver acetate to water is much lower (1 g/100 mL at 20 °C) than that of silver nitrate (219 g/100 mL at 20 °C), and for a fair comparison we synthesize the two Ag-MC15 films using the same wt% of silver nitrate and silver acetate. The FTIR spectra of those films are shown in Figs. 6e and 6f, respectively. To compare Figs. 6e and 6f with Fig. 6b, we must bear in mind that the wt% of silver nitrate and silver acetate with respect to MC15 we employ to synthesize the Ag-MC15 films for Figs. 6e and 6f is much lower than that of the Ag-MC15 film we employ for Fig. 6b. The additional peak at 1318 cm^{-1} we observe in the Ag-MC15 films synthesized using silver nitrate (Figs. 6e and 6b) does not appear in the Ag-MC15 film synthesized using silver acetate (Fig. 6f). This implies that the peak at 1318 cm^{-1} must be associated with a certain vibrational mode associated with nitrate or nitrogen, and it is most likely the N-O stretching mode of NO_3^- [43].

Antibacterial test

We investigate the antibacterial property of the Ag-MC films using the agar diffusion test against *E. coli*. The photos of the antibacterial tests with the Ag-MC15 and Ag-MC400 films under the different laser irradiation conditions are shown in Fig. 7a. Of course there is no inhibited zone for the pure MC15 and MC400 films, as shown in films E and J of Fig. 7a. To be more quantitative, we present the histograms of the inhibited areas [41], and the results with the Ag-MC15 films are shown in Figs. 7b. Interestingly, Fig. 7b shows that, (1) for the given laser power the film prepared by the shorter irradiation time has a stronger antibacterial property, while (2) for the given irradiation time the film prepared by the lower laser power

has a stronger antibacterial property. To understand these results, we note that there are two factors that determine the antibacterial property of the films. The first one is the *number of remaining Ag+ ions* left in the film after the CO_2 laser irradiation. The fact that film A (30 sec irradiation at 0.8 W) has a stronger antibacterial property than film B (90 sec irradiation at 0.8 W) implies that the remaining Ag^+ ions rather than the synthesized Ag NPs in the film does a better job to kill the bacteria. The second one is the *number and size* of Ag NPs in the film. Since most of the Ag^+ ions in the MC15 film have been reduced to Ag NPs after the laser irradiation of 30 sec at 1 W as we have explained in section 3.2, we may assume that there are
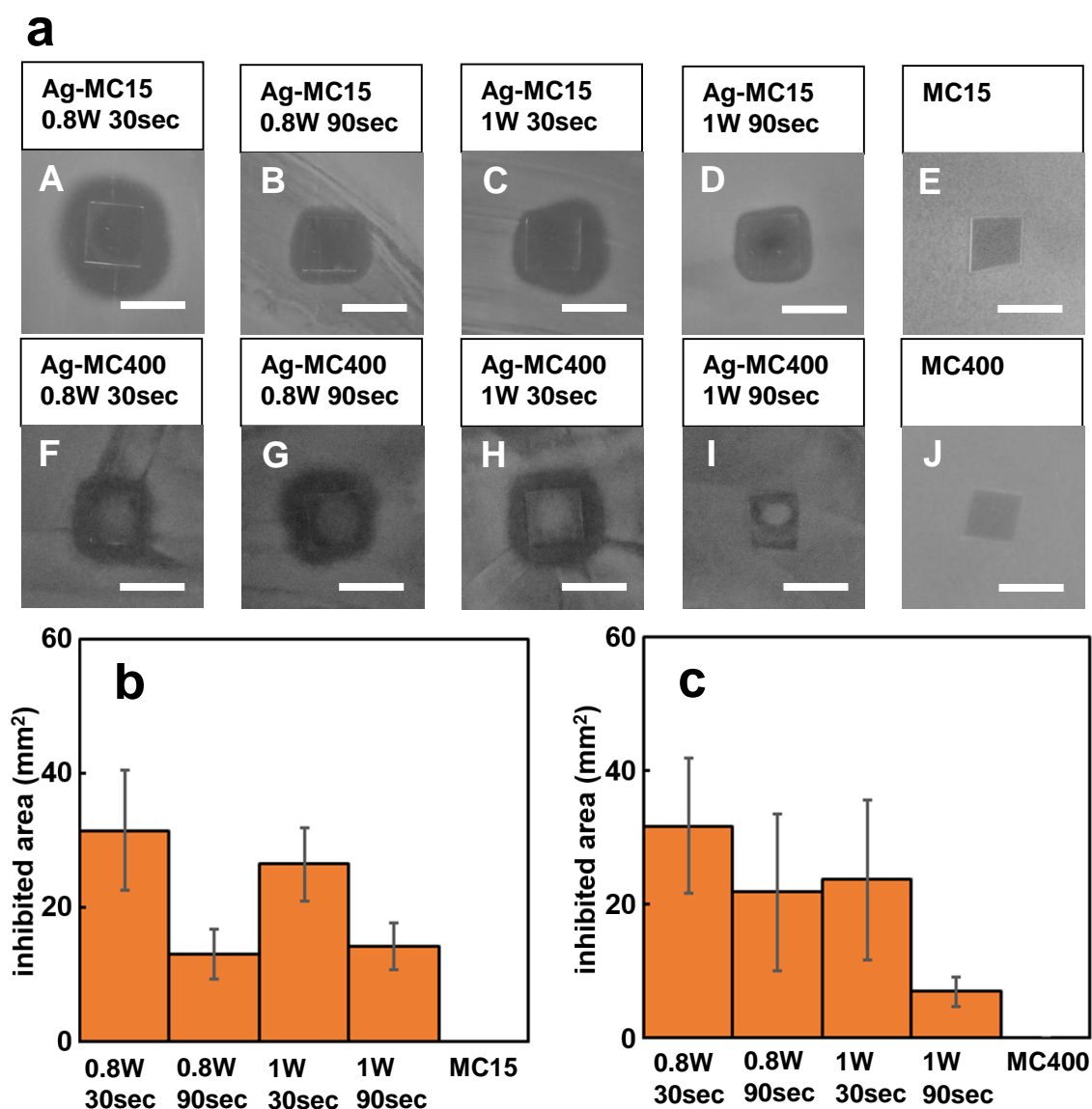

Figure 7 (a) Photos for the antibacterial test with the 4 mm × 4 mm Ag-MC15 and Ag-MC400 films synthesized under the different laser irradiation conditions. The inhibited areas around the Ag-MC15 and Ag-MC400 films are shown in (b) and (c) with the results of control samples, MC15 and MC400 films. All scale bars in (a) represent 5 mm.

very few Ag^+ ions left in both films C and D. But the results in Fig. 7a show that film C has a stronger antibacterial property than film D. This is because the *total surface area* of Ag NPs in film C (with average NPs size of 30.6 nm) is larger than that in film D (with average NP size of 37.6 nm), as we can infer from Figs. 4a and 4b, and accordingly more Ag atoms at the surface of Ag NPs in film C can presumably release electrons to become Ag^+ ions. Similar results are presented in Fig. 7c with the Ag-MC400 films. Interestingly, a comparison of Figs. 7b and 7c suggest that the antibacterial property of the Ag-MC400 films (30 sec irradiation at 0.8 W, 90 sec irradiation at 0.8 W, and 30 sec irradiation at 1 W) is more or less similar to that of the Ag-MC15 film under the corresponding laser irradiation conditions. To find a reason for this we note that the peak values of absorbance of the Ag-MC15 (90 sec irradiation at 0.8 W and 30 sec irradiation at 1 W) films are all about 2.3 (Fig. 2) while those of Ag-MC400 films (30 sec irradiation at 0.8 W, 90 sec irradiation at 0.8 W, and 30 sec irradiation at 1 W) are about 2.4, 2.6, and 2.7 (Fig. 3). This means that the number of Ag NPs in the Ag-MC400 films is about a factor of two more than that in the Ag-MC15 films, i.e., $10^{-2.3}/10^{-2.6} \sim 2$. We also recall that the thicknesses of Ag-MC15 and Ag-MC400 films are 440 and 820 nm, respectively, and hence the thickness of the latter is about 1.86 times more than that of the former. By combining those facts we can conclude that the number density of Ag NPs in the Ag-MC400 films are seemingly slightly more than those in the Ag-MC15 films, which may result in slightly more Ag^+ ions. It is not easy, however, to pinpoint the reason, since the thicknesses of Ag-MC15 and Ag-MC 400 films are different. The only thing we can surely say for the results with the Ag-MC400 films is that the antibacterial property of film I (90 sec irradiation at 1 W) is significantly weaker than the others, because the size of Ag NPs are far larger than the others (Fig. 5b), and accordingly the total surface area of Ag NPs in film I is far less than the others, which means that a far smaller number of Ag^+ ions can be released from the Ag NPs in film I.

Conclusions

In conclusion we have studied the influence of the polymer molecular weight on the properties of in-situ synthesized silver-methylcellulose nanocomposite films using a CO_2 laser. Although the reduction power of methylcellulose with a larger molecular weight has been found to be weaker than that with a smaller molecular weight in the solution phase, it is not so weak when it is in the matrix phase, presumably because the residual water molecules in the former film helps Ag^+ ions to have better mobility in the polymer matrix to promote the reduction. From

the UV-vis spectra and SEM images of the synthesized films we have found that the silver nanoparticles synthesized in the methylcellulose matrix with a larger molecular weight tends to aggregate to form larger nanoparticles, since the nanoparticles cannot move so much in the more viscous methylcellulose matrix. Moreover, we have found that the additional peak in the FTIR spectra of the nanocomposite films is associated with the nitrate group, and it is most likely the N-O stretching mode of NO_3^-, since the silver-methylcellulose film prepared with silver acetate instead of silver nitrate does not show such a peak. We have also carried out the antibacterial test of the nanocomposite films synthesized under the different laser powers and irradiation times. The difference of antibacterial property is roughly and qualitatively explained by the number of remaining Ag^+ ions and the effective surface area of silver nanoparticles. Our results suggest that the choice of the molecular weight of the matrix polymer influences the various properties of the synthesized silver-methylcellulose nanocomposite films, and the similar must be true for any polymer-based nanocomposites.

Acknowledgments

1. Sih BC, Wolf MO (2005) Metal nanoparticle — conjugated polymer nanocomposites. Chem Commun 27:3375–3384. https://doi.org/10.1039/b501448d

2. Ramesh G V, Porel S, Radhakrishnan TP (2009) Polymer thin films embedded with in situ grown metal nanoparticles. Chem Soc Rev 38:2646–2656. https://doi.org/10.1039/b815242j

3. Faupel F, Zaporojtchenko V, Strunskus T, Elbahri M (2010) Metal-polymer nanocomposites for functional applications. Adv Eng Mater 12:1177–1190. https://doi.org/10.1002/adem.201000231

4. Mbhele ZH, Salemane MG, Sittert CGCE Van, et al (2003) Fabrication and Characterization of Silver - Polyvinyl Alcohol Nanocomposites. Chem Mater 15:5019–5024

5. Khanna PK, Singh N, Charan S, et al (2005) Synthesis and characterization of Ag/PVA nanocomposite by chemical reduction method. Mater Chem Phys 93:117–121. https://doi.org/10.1016/j.matchemphys.2005.02.029

6. Xu P, Han X, Zhang B, et al (2014) Multifunctional polymer – metal nanocomposites via direct chemical reduction by conjugated polymers. Chem Soc Rev 43:1349–1360. https://doi.org/10.1039/c3cs60380f

7. Pucci A, Bernabo M, Elvati P, et al (2006) Photoinduced formation of gold nanoparticles into vinyl alcohol based polymers. J Mater Chem 16:1058–1066. https://doi.org/10.1039/b511198f

8. Sakamoto M, Tachikawa T, Fujitsuka M, Majima T (2006) Acceleration of Laser-Induced Formation of Gold Nanoparticles in a Poly (vinyl alcohol) Film. Langmuir 22:6361–6366

9. Lee CJ, Karim MR, Lee MS (2007) Synthesis and characterization of silver / thiophene nanocomposites by UV-irradiation method. Mater Lett 61:2675–2678. https://doi.org/10.1016/j.matlet.2006.10.021

10. Sakamoto M, Fujistuka M, Majima T (2009) Light as a construction tool of metal nanoparticles : Synthesis and mechanism. J Photochem Photobiol C Photochem Rev 10:33–56. https://doi.org/10.1016/j.jphotochemrev.2008.11.002

11. Jiang T, Li J, Zhang L, et al (2014) Microwave assisted in situ synthesis of Ag-NaCMC films and their reproducible surface-enhanced Raman scattering signals. J Alloys Compd 602:94–100

12. Porel S, Singh S, Harsha SS, et al (2005) Nanoparticle-Embedded Polymer : In Situ Synthesis , Free-Standing Films with Highly Monodisperse Silver Nanoparticles and Optical Limiting. Chem Mater 17:9–12

13. Kashihara K, Uto Y, Nakajima T (2018) Rapid in situ synthesis of polymer-metal nanocomposite films in several seconds using a CO2 laser. Sci Rep 8:14719. https://doi.org/10.1038/s41598-018-33006-9

14. Moon RJ, Martini A, Nairn J, et al (2011) Cellulose nanomaterials review : structure, properties and nanocomposites. Chem Soc Rev 40:3941–3994. https://doi.org/10.1039/c0cs00108b

15. Hoeng F, Denneulin A, Bras J (2016) Use of nanocellulose in printed electronics : a review. Nanoscale 8:13131–13154. https://doi.org/10.1039/c6nr03054h

16. Rie J Van, Thielemans W (2017) Cellulose–gold nanoparticle hybrid materials. Nanoscale 9:8525–8554. https://doi.org/10.1039/c7nr00400a

17. Zhang BT, Wang W, Zhang D, et al (2010) Biotemplated Synthesis of Gold Nanoparticle – Bacteria Cellulose Nanofiber Nanocomposites and Their Application in Biosensing. Adv Funct Mater 20:1152–1160. https://doi.org/10.1002/adfm.200902104

18. Yan W, Chen C, Wang L, et al (2016) Facile and green synthesis of cellulose nanocrystal-supported gold nanoparticles with superior catalytic activity. Carbohydr Polym 140:66–73

19. Koga H, Tokunaga E, Hidaka M, et al (2010) Topochemical synthesis and catalysis of metal nanoparticles exposed on crystalline cellulose nanofibers. Chem Commun 46:8567–8569. https://doi.org/10.1039/c0cc02754e

20. Li X, Chen S, Hu W, et al (2009) In situ synthesis of CdS nanoparticles on bacterial cellulose nanofibers. Carbohydr Polym 76:509–512. https://doi.org/10.1016/j.carbpol.2008.11.014

21. Li R, He M, Li T, Zhang L (2015) Preparation and properties of cellulose / silver nanocomposite fibers. Carbohydr Polym 115:269–275. https://doi.org/10.1016/j.carbpol.2014.08.046

22. Liou P, Xavier F, Kong F, et al (2017) Cellulose nanofibers coated with silver nanoparticles as a SERS platform for detection of pesticides in apples. Carbohydr Polym 157:643–650. https://doi.org/10.1016/j.carbpol.2016.10.031

23. Galland S, Andersson RL, Salajkova M, et al (2013) Cellulose nanofibers decorated with magnetic nanoparticles – synthesis , structure and use in magnetized high toughness membranes for a prototype loudspeaker. J Mater Chem C 1:7963–7972. https://doi.org/10.1039/c3tc31748j

24. Lukach A, Therien-Aubin H, Querejeta-Fernandez A, et al (2015) Coassembly of Gold Nanoparticles and Cellulose Nanocrystals in Composite Films. Langmuir 31:5033–5041. https://doi.org/10.1021/acs.langmuir.5b00728

25. Bhui DK, Pyne S, Sarkar P, et al (2011) Temperature controlled synthesis of silver nanostructures of variable morphologies in aqueous methyl cellulose matrix. J Mol Liq 158:170–174. https://doi.org/10.1016/j.molliq.2010.11.014

26. Mahanta N, Valiyaveettil S (2012) In situ preparation of silver nanoparticles on biocompatible methacrylated poly (vinyl alcohol) and cellulose based polymeric nanofibers. RSC Adv 2:11389–11396. https://doi.org/10.1039/c2ra20637d

27. Kumar A, Negi YS, Bhardwaj NK, Choudhary V (2012) Synthesis and characterization of methylcellulose/PVA based porous composite. Carbohydr Polym 88:1364–1372. https://doi.org/10.1016/j.carbpol.2012.02.019

28. Maity D, Mollick MMR, Mondal D, et al (2012) Synthesis of methylcellulose-silver nanocomposite and investigation of mechanical and antimicrobial properties. Carbohydr Polym 90:1818–1825. https://doi.org/10.1016/j.carbpol.2012.07.082

29. Xu W, Xu Q, Huang Q, et al (2015) Electrically conductive silver nanowires- filled methylcellulose composite transparent films with high mechanical properties. Mater Lett 152:173–176. https://doi.org/10.1016/j.matlet.2015.03.111

30. Nasatto PL, Pignon F, Silveira JLM, et al (2015) Methylcellulose, a cellulose derivative with original physical properties and extended applications. Polymers (Basel) 7:777–803. https://doi.org/10.3390/polym7050777

31. Aziz SB, Rasheed MA, Ahmed HM (2017) Synthesis of Polymer Nanocomposites Based on [Methyl Cellulose](1-x):(CuS)x(0.02M<x<0.08M) with Desired Optical Band Gaps. Polymers (Basel) 9:194. https://doi.org/10.3390/polym9060194

32. Kolarova K, Samec D, Kvitek O, et al (2017) Preparation and characterization of silver nanoparticles in methyl cellulose matrix and their antibacterial activity. Jpn J Appl Phys 56:. https://doi.org/10.7567/JJAP.56.06GG09

33. Nunes MR, de Souza Maguerroski Castilho M, de Lima Veeck AP, et al (2018) Antioxidant and antimicrobial methylcellulose films containing Lippia alba extract and silver nanoparticles. Carbohydr Polym 192:37–43. https://doi.org/10.1016/j.carbpol.2018.03.014

34. Chen J, Wang J, Zhang X, Jin Y (2008) Microwave-assisted green synthesis of silver nanoparticles by carboxymethyl cellulose sodium and silver nitrate. Mater Chem Phys 108:421–424. https://doi.org/10.1016/j.matchemphys.2007.10.019

35. Rangelova N, Aleksandrov L, Angelova T, et al (2014) Preparation and characterization of SiO2/CMC/Ag hybrids with antibacterial properties. Carbohydr Polym 101:1166–1175

36. Shi D, Wang F, Lan T, et al (2016) Convenient fabrication of carboxymethyl cellulose electrospun nanofibers functionalized with silver nanoparticles. Cellulose 23:1899–1909. https://doi.org/10.1007/s10570-016-0918-x

37. Park JS, Kim T, Kim WS (2017) Conductive Cellulose Composites with Low Percolation Threshold for 3D Printed Electronics. Sci Rep 7:3246. https://doi.org/10.1038/s41598-017-03365-w

38. Cheng F, Betts JW, Kelly SM, et al (2013) Synthesis and antibacterial effects of aqueous colloidal solutions of silver nanoparticles using aminocellulose as a combined reducing and capping reagent. Green Chem 15:989–998. https://doi.org/10.1039/c3gc36831a

39. Saha NR, Sarkar G, Roy I, et al (2016) Nanocomposite films based on cellulose acetate/polyethylene glycol/modified montmorillonite as nontoxic active packaging material. RSC Adv 6:92569–92578. https://doi.org/10.1039/C6RA17300D

40. Luo C, Zhang Y, Zeng X, et al (2005) The role of poly(ethylene glycol) in the formation of silver nanoparticles. J Colloid Interface Sci 288:444–448. https://doi.org/10.1016/j.jcis.2005.03.005

41. Ruparelia JP, Chatterjee AK, Duttagupta SP, Mukherji S (2008) Strain specificity in antimicrobial activity of silver and copper nanoparticles. Acta Biomater 4:707–716. https://doi.org/10.1016/j.actbio.2007.11.006

42. Suflet DM, Chitanu GC, Popa VI (2006) Phosphorylation of polysaccharides: New results on synthesis and characterisation of phosphorylated cellulose. React Funct Polym 66:1240–1249. https://doi.org/10.1016/j.reactfunctpolym.2006.03.006

43. Silverstein RM, Webster FX., Kiemle DJ., Bryce DL (2014) Spectrometric Identification of Organic Compounds. Wiley

{Bibliography}